

Experimental Study of Few-Layer Graphene: Optical Anisotropy and Pseudo-Brewster Angle Shift in Vacuum Ultraviolet Spectral Range

Nadeem Ahmed Malik,* Piergiorgio Nicolosi, Kety Jimenez, Ahmed Gaballah, Angelo Giglia, Marco Lazzarino, and Paola Zuppella*

The optical properties of mono- and trilayer graphene on SiO₂/Si substrate are studied at hydrogen Lyman-alpha (121.6 nm) spectral line for the first time. The optical anisotropy of graphene at this wavelength is experimentally demonstrated by retrieving the anisotropic "effective" optical constants. The results confirm that the axis of symmetry is nearly perpendicular to the surface and coherently related to the π -orbitals' structural orientation. Furthermore, it is observed that graphene strongly affects the performances of the substrate by inducing a pseudo-Brewster angle downshift, which depends on the number of graphene layers. This finding is in contrast with what occurs in the visible spectral range, where the upshift of the pseudo-Brewster angle is experienced in similar samples.

As far as optical applications are concerned, hostile working conditions are those in which the optical systems and the samples experience debris and ion flow, humidity, thermal and mechanical shocks, and strong thermal load. Such a stress is common to many application fields, including space instrumentation, lithographic systems, third- and fourth-generation radiation sources, and pump and probe experiments with intense, ultrashort pulses.

Whatever the application in optics, the determination of the optical constants, the optical absorption, and the polarization effects are some of the properties that

1. Introduction

A perfect sheet of graphene is a very thin layer of sp^2 -hybridized carbon atoms arranged in a bidimensional hexagonal lattice without surface defects.^[1,2] This structure determines the characteristics that have made it successful, including high thermal and electrical conductivity, semimetallic behavior, and extreme robustness and stiffness.^[3-7] It should be noted that graphene also exhibits excellent chemical and thermal stability and the arrangement of the carbon atoms makes it inert and impermeable to all atomic species including helium.^[6] For these reasons, it is an outstanding candidate as a protective layer to be used in the development of optical components devoted to operate in harsh environments.^[4,7]


deserve to be deeply investigated before using graphene for an optical device.

Several theoretical and experimental studies predict the optical response of graphene in the visible (VIS) and near-infrared (NIR) spectral ranges.^[8,9] We know, to date, that a single layer of graphene absorbs about 2.3% of the incident light at the VIS–NIR wavelengths.^[10] A significant number of scientists have determined the VIS–NIR optical constants of graphene,^[11-15] but the results strongly depend on the deposition and growth method, purity, oxidation, transfer, and interactions with the substrate.^[16,17]

Despite the large number of studies in the VIS–NIR, there is a lack in the vacuum ultraviolet (VUV) and extreme ultraviolet

Dr. N. A. Malik, Prof. P. Nicolosi, Dr. K. Jimenez
Department of Information Engineering
University of Padova
Padova 35131, Italy
E-mail: nadeemahmed.malik@phd.unipd.it, nadeem7_qau@yahoo.com

Dr. N. A. Malik, Prof. P. Nicolosi, Dr. K. Jimenez, Dr. P. Zuppella
Istituto di Fotonica e Nanotecnologie-Consiglio Nazionale delle Ricerche (IFN-CNR)
Padova, Italy
E-mail: paola.zuppella@pd.ifn.cnr.it

 The ORCID identification number(s) for the author(s) of this article can be found under <https://doi.org/10.1002/adpr.202000207>.

© 2021 The Authors. Advanced Photonics Research published by Wiley-VCH GmbH. This is an open access article under the terms of the Creative Commons Attribution License, which permits use, distribution and reproduction in any medium, provided the original work is properly cited.

DOI: 10.1002/adpr.202000207

Dr. K. Jimenez
Department of Physics
Universidad Autonoma de Santo Domingo
Santo Domingo 10105, Dominican Republic

Dr. A. Gaballah
Photometry and Radiometry Division
National Institute of Standards (NIS)
Giza 12211, Egypt

Dr. A. Giglia
Istituto Officina dei Materiali-Consiglio Nazionale delle Ricerche (IOM-CNR)
Trieste, Italy

Dr. M. Lazzarino
Laboratorio TASC
Istituto Officina dei Materiali-Consiglio Nazionale delle Ricerche (IOM-CNR)
Trieste, Italy

(EUV) spectral region. The purpose of the present study is to fill this gap to explore graphene's potentiality in this spectral range.

In this scenario, we have studied the reflectance response of few-layer graphene at hydrogen Lyman-alpha (121.6 nm) spectral line, with the precise aim of determining its optical constants, the effects induced on the substrate performances, and the possible polarizing effects. We have investigated the s- and p-polarized reflectance of the samples, shift of the pseudo-Brewster angle, determination of the optical constants, and experimental evidence of optical anisotropy linked to the planar structure of graphene and spatial distribution of the π -orbitals. These kinds of measurements have required the use of VUV–EUV reflectometry^[18] and large-scale facilities as synchrotron.^[19,20] The physical and chemical quality, purity, and morphology of the samples have been also characterized to fully describe the types of samples for which the optical properties were then determined.

As far as we know, it is the first time that these analyses are presented for graphene at VUV wavelengths, opening a concrete perspective to new and uncharted applications.

The first part of the article is devoted to the technical description of the measurements and analysis methods and the last one to the discussion of the data, results, and outlook.

2. Experimental Section

The samples under investigation were commercial specimens fabricated by Graphenea Inc.^[21] They consisted of a bulky layer of silicon dioxide deposited onto $10 \times 10 \text{ mm}^2$ Si substrate and capped by graphene, as shown in **Figure 1**. Graphene was grown by chemical vapor deposition (CVD) on an $18 \mu\text{m}$ -thick copper foil and then transferred to SiO_2 (285 nm)/Si. In case of the 3LG, a multiple-transfer sequence was applied.^[21,22] They were standard samples, as the oxide thickness was optimized at 280–300 nm to guarantee the optical contrast for optical microscope (OM) observations.^[23,24] The OM analysis is qualitative: it allows to identify regions with a larger number of graphene layers and distinguish almost “by eye” wrinkled areas determined by the transfer process and the adhesion of graphene on the substrate.^[25] High-resolution microscopies, such as

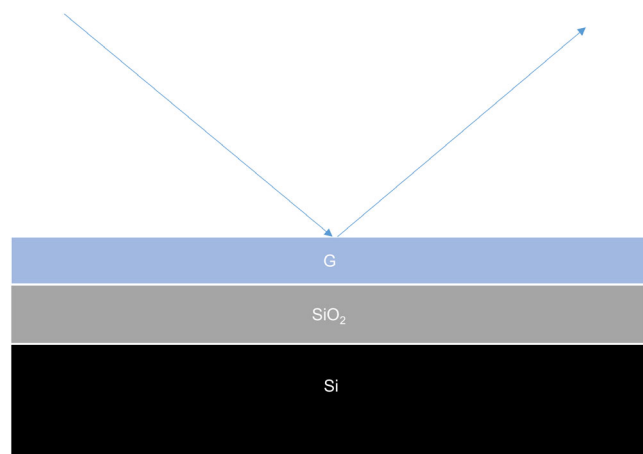


Figure 1. Structure of the samples: graphene layer onto SiO_2 (285 nm)/Si substrate. The thickness of graphene depends on the number of layers.

atomic force microscopy (AFM), allow the quantitative measurement of the thickness and size of discontinuous graphene islands.^[26]

In detail, the samples that we measured were 1LG/ SiO_2 (285 nm)/Si, 3LG/ SiO_2 (285 nm)/Si, and SiO_2 /Si, the last one as reference.

The surface morphology of the samples was investigated by AFM in no-contact mode operation (Park System XE-70).^[27] The chemical quality of the coating was tested by Raman and X-ray photoelectron spectroscopy (XPS).

The Raman set-up available at CNR-IOM was based on three laser beams emitting at 532 nm with beam widths of 2 MHz (Cobolt Samba), 660 nm–1 MHz (Quantum-Laser Torus), and 785 nm–50 MHz (IO Matchbox), respectively, an upright Olympus microscope with high NA objective (up to 8.8 with maximum spatial resolution of 330 nm), and a 330 mm monochromator equipped with an LN_2 -cooled charge-coupled device (CCD) camera (Acton 330i and Princeton Instr) and a 750 mm monochromator equipped with an electron multiplying charge-coupled device (EMCCD) camera (Shamrock SR750 and Newton, Andor-Solis). For graphene quality evaluation, we used the 532 nm excitation wavelength, which allowed a more straightforward comparison with literature data. Raman scattering is a useful technique to determine doping, quality, and number of layers of graphene.^[28–35] Generally, there are three main peaks in the Raman spectra of graphene: *D*, *G*, and *2D*. The intensity of those and the ratios *D/G* and *2D/G* give information about the crystalline quality and defects density on the graphene matrix.

The XPS measurements were carried out at BEAR beamline (ELETTRA synchrotron-Trieste). Standard gold sample was used for calibration, and a broad scan was conducted in the binding energy (BE) range of 50–650 eV. High-resolution *C1s* scan at 275–305 eV BE was measured for graphene. CasaXPS software was used for the analysis of the XPS data.^[36] The peak fitting was done after background subtraction for which we used the technique based on the Shirley method.

The optical characterizations of the samples were conducted at hydrogen Lyman alpha using a VUV–EUV laboratory-based reflectometer (CNR-IFN, Padova) and synchrotron light facilities (BEAR beamline-ELETTRA synchrotron-Trieste).^[19] The VUV–EUV reflectometer equipment available in Padova was a Johnson–Onaka normal-incidence monochromator coupled with a deuterium spectral lamp (Hamamatsu, L2D2), as shown in **Figure 2**.

The toroidal grating mounted on the reflectometer was Pt coated with 600 lines/mm. Monochromatic radiation was condensed on the sample by a toroidal mirror working at 45° incidence angle. The samples were placed in the experimental chamber on a rotating holder to change the incidence angle. The detector was a channel electron multiplier (CEM KBL 10RSR).^[37] The angular reflectance measurements of the samples were recorded for two mutually orthogonal orientations of the plane of incidence. From the experimental data and by knowing the polarization degree of the incidence beam, we retrieved the reflectance R_s and R_p corresponding to s- and p-polarized light. The detailed procedure is described in the study by Gaballah et al.^[38] The same apparatus was recently implemented with a rotating polarizer for ellipsometry in

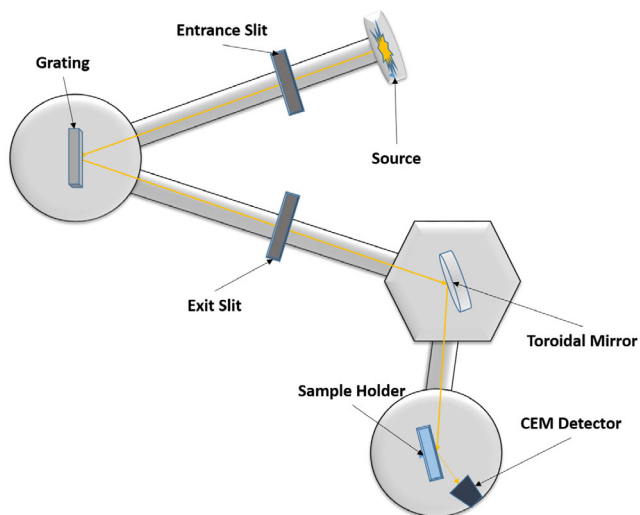


Figure 2. Schematic view of the laboratory-based VUV–EUV reflectometer used for the optical characterization of the samples.

VUV–EUV spectral region.^[18,39] The technical data of the system and the method are described in studies by Gaballah et al.^[38,40]

BEAR beamline (ELETTRA synchrotron-Trieste) operated in the 2.8–1600 eV (443–0.775 nm) spectral region, delivering polarized light of selectable ellipticity, from nearly linear to elliptical. The available spectroscopic tools included specular reflectivity and XPS equipment,^[19,20] which we used in this experiment. The angular reflectance measurements of the specimens were carried out for two mutually orthogonal orientations of the plane of incidence, and, as in case of in-house facility, the reflectance R_s and R_p were retrieved by knowing the polarization degree of the incident beam.

The experimental reflectance curves were fitted using IMD software to estimate the optical constants of graphene.^[41] IMD is a software written in the IDL language, a powerful tool for modeling the optical properties of multilayer stacks. The software recursively applies the Fresnel equations to a simple multilayer model that assumes homogeneous layers with parallel interfaces. IMD uses the CURVEFIT procedure, an adaptation of the Marquardt algorithm included in the IDL library, to estimate unknown parameters values.^[41]

3. Results

The surface morphology of the samples was studied by using the Park System 70 XE-series AFM available at (CNR-IFN) Padova, Italy. Surface morphology scans of different areas were conducted for different locations of the samples in noncontact mode. The root-mean-square (RMS) and average surface roughness (R_a) were determined using XEI data analysis software (Park Systems Corp). **Figure 3** shows a $5 \times 5 \mu\text{m}$ scan area of 1LG sample. The morphology appears quite uniform, although some wrinkles are present in the surface. The wrinkles formation might occur during cooling in the CVD process because of the different thermal expansion coefficients of graphene and metal substrate or during the transfer process because of the surface morphology

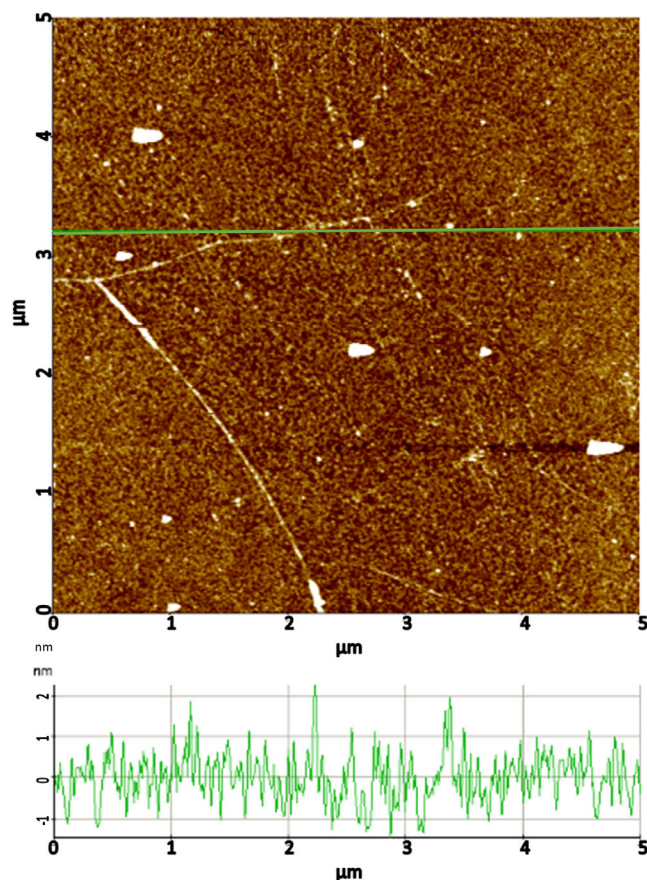


Figure 3. Atomic force microscope image ($5 \times 5 \mu\text{m}$) of 1LG/SiO₂/Si recorded in noncontact mode. The 2D image shows the morphology of the sample; the profile on the bottom corresponds to the green line.

mismatch between the growth substrate and the SiO₂/Si final transfer substrate.

The surface quality of the samples strongly depends on the number of graphene layers because the multiple-transfer process increases the defects and the wrinkles. These effects are especially evident in **Figure 4** that shows the surface morphology of the 3LG/SiO₂/Si sample. In quantitative terms, the roughness R_q of 1LG is $0.80 \pm 0.02 \text{ nm}$, whereas in case of 3LG, the roughness R_q is $4.30 \pm 0.02 \text{ nm}$.

The quality of 1LG is guaranteed by the manufacturer, which reports the Raman analysis,^[26] whereas the quality of 3LG was investigated by Raman spectroscopy in the laboratory (Trieste-Basovizza-IOM). The results of the measurements are shown in **Figure 5**. The sample was analyzed in four different regions (P1, P2, P3, and P4) and the results show the characteristic peaks (*D*, *G*, and 2*D*) of graphene. The intensity of *G* and 2*D* peaks depends on the investigated region as well the ratio 2*D*/*G*, that ranges between 1.44 and 1. These evidences confirm that the multilayer graphene film covering the substrate is not homogeneous as expected and the 3LG is not guaranteed over the whole surface. However, the small *D* peak intensity and the small ratio *D*/*G* confirm that the *sp*³ defects are negligible.

Aware that it is not easy to obtain a homogeneous 3LG coating, we have completed the full characterization of the 3LG sample by

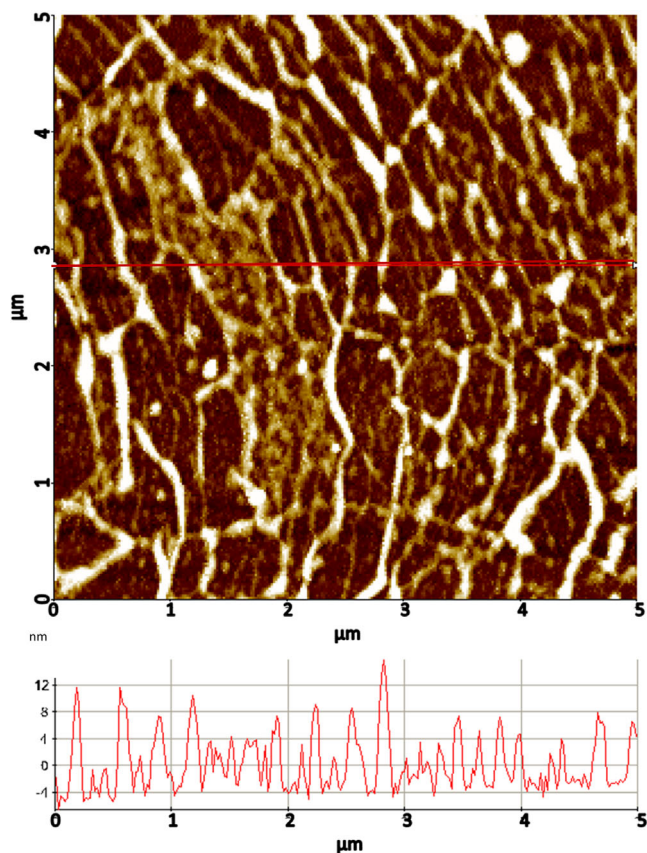


Figure 4. Atomic force image ($5 \times 5 \mu\text{m}$) of 3LG/SiO₂/Si recorded in noncontact mode. The 2D image shows the morphology of the sample; the profile on the bottom refers to the red line.

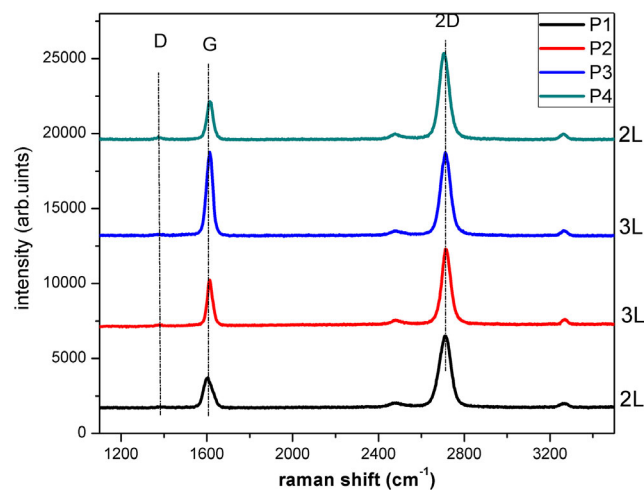


Figure 5. Raman spectra of 3LG/SiO₂/Si sample. The measurements have been carried out at four different regions (P1, P2, P3, and P4) of the specimen. Raman scan of each region is represented with different colors.

XPS analysis. XPS spectroscopy was conducted at BEAR beamline. High-resolution C1s scan was recorded (280–305 eV). The detailed measurement parameters are shown in the Table 1.

Table 1. XPS measurement parameters.

XPS C1s scan parameters	
Photon energy [eV]	400
Initial K.E [eV]	95
Final K.E [eV]	120
ΔE [eV]	0.038

To interpret the measured spectra in terms of quality of graphene samples, chemical groups present, a well-known technique of deconvolution of XPS data was used. To take into account the inelastic photoelectron, Shirley's background was removed from the spectra. The well-known CasaXPS software was used for the analysis of the XPS data.^[36] Figure 6 shows the spectra. The spectrum in Figure 6 exhibits the strong prevalence of the peak (C–C) related to characteristic sp^2 -hybridized carbon atoms of graphene. The convolution and fitting of the data also reveal some small contribution of (C–O–C) sp^3 structure at a higher BE (286 eV). These results are compliant with the Raman spectra outcomes.

Figure 7 shows the s- and p-reflectance curves of 1LG/SiO₂/Si, 3LG/SiO₂/Si and SiO₂/Si specimens. All the samples were measured at BEAR beamline and the reflectance R_s and R_p retrieved from the experimental data, as it is explained in the previous section. The angular step was 1° for the 1LG/SiO₂/Si sample (R_s red line and R_p magenta line) and 0.5° in case of 3LG/SiO₂/Si (R_s black line and R_p grey line). For both specimens, the uncertainty associated with the reflectance is 10% in 5° – 15° angular range and 5% in 15.5° – 85° . The associated errors were calculated by applying the error propagation formula.^[42]

In case of 1LG/SiO₂/Si, the measurements were also carried out at CNR-IFN with angular steps of 10° and 5° (R_s cyan triangles and R_p cyan dots) depending on the angular region. Figure 7 shows both data showing a good agreement between synchrotron and laboratory measurements, except at grazing-incidence angles, where the alignment of the sample and the

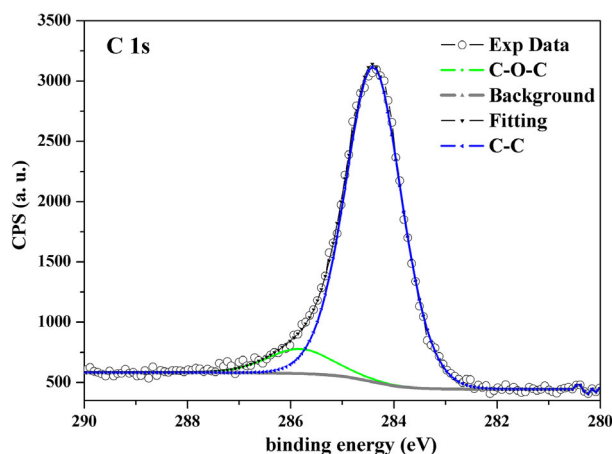


Figure 6. X-ray photoelectron (C1s) spectra of 3LG sample measured at BEAR beamline. The experimental data are reported with the fitting, resulting in the underlying contributions due to C–O–C and C–C bonds. The background line is also shown.

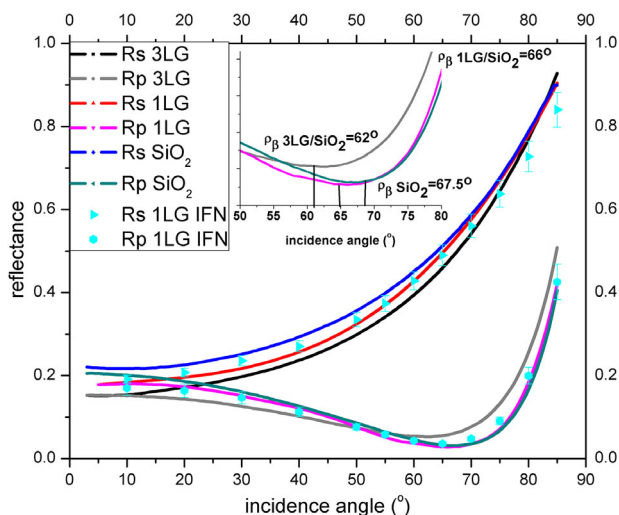


Figure 7. Reflectance measurements (s- and p-polarization) taken at BEAR of 1LG/SiO₂/Si (R_s red line and R_p magenta line), 3LG/SiO₂/Si (R_s black line and R_p grey line), and SiO₂/Si (R_s blue line and R_p green line) specimens. The inset shows the p-reflectance curves and shift of the pseudo-Brewster angle in case of 1LG and 3LG on top of SiO₂. R_s cyan triangles and R_p cyan dots refer to measurements of 1LG/SiO₂/Si recorded at IFN.

nonuniformity of the CEM affect the in-house measurements by adding a slight displacement from the BEAR data and increasing the uncertainty. The plot includes also the measurements of SiO₂ (R_s blue line and R_p green line).

We need to introduce the concept of the pseudo-Brewster angle to explain what we have experimentally observed. In case of absorptive materials, the Brewster angle is generalized, and we refer to pseudo-Brewster angle. The pseudo-Brewster angle corresponds to the minimum of the p-reflectance. This occurs when the angle between the reflected and transmitted beams is 90° and the direction of the reflected beam is parallel to the axis of the equivalent oscillating dipoles in the region below the surface interface, where both the reflected and the transmitted waves originate. In the VUV–EUV spectral range, most of the materials are absorptive and, for those, the reflected beam is never totally extinguished, generating a pseudo-Brewster angle.

The first interesting finding that we immediately note is that the graphene layers on top of the SiO₂ induce a decrease in s-reflectance and a sort of downshift of the pseudo-Brewster angle. We have used the synchrotron data for determining the pseudo-Brewster angle positions and the optical constants. The estimated downshift is 1.5° in case of 1LG and 5° in case of 3LG, as shown in the inset of Figure 7. It means that the minimum of the p-reflectance curves moves toward smaller incidence angles as the number of layers increases.

On the contrary, the effect of graphene layer on top of SiO₂ is the shift of the pseudo-Brewster angle to larger values in the visible range.^[43,44]

We need to analyze the interaction of graphene with light to understand the phenomenon. Graphene layer is the basic element of hexagonal graphite. The 2D layered structure determines the large anisotropic optical properties of graphite. The problem

was well addressed in the study by Marinopoulos,^[45] where the authors have derived the optical absorption of graphene for photon energy ranging from 0 to 30 eV. The optical absorption is directly related to the interaction of the electromagnetic wave with the sample and depends on the dipole oscillator moment relative to the transition and, consequently, on the band structure and relative density of state of the material. A strong absorption corresponds to a large energy transfer between the beam and the material. Figure 4 and 5 in the study by Marinopoulos^[45] shows the optical absorption of graphene for oscillating fields parallel and orthogonal to the surface of the sample. In case of the parallel component, the absorption shows two contributions, one in the range 0–5 eV photon energy, peaked in the range of 10–30 eV peaked at about 14 eV. These correspond, respectively, to π – π^* and σ – σ^* interband transitions. For the perpendicular component, the absorption spectrum is very weak for low-energy photons, below 5 eV, and shows strong peaks in the range above 10 eV. These correspond to π – σ^* and σ – π^* transitions according to the selection rules.

Figure 8 shows the pseudo-Brewster angle conditions in three cases.

- 1) SiO₂/Si in the VUV and visible spectral range;
- 2) #LG/SiO₂/Si in the visible range;
- 3) #LG/SiO₂/Si in the VUV range.

In the visible range, the photon energy is relatively low and the polarization component with electric field parallel to the graphene layer strongly interacts and induces a dipole component, P'_G , mostly parallel to the surface, (see “visible range” sketch of Figure 8). This effect superimposed with the dipole component in the SiO₂ substrate, P_{bulk} , generates a rotated P'_{tot} and justifies the relative shift of the pseudo-Brewster angle to larger values.^[44]

On the contrary, for relatively large-energy photons, like at about 10 eV and above, both polarizations, perpendicular and parallel to the graphene layer surface, interact. This gives rise to a dipole component, P'_G , oscillating in a direction slightly rotated, as we can observe in the VUV range sketch of Figure 8 (red arrow). The P''_G component superimposed to the dipole P_{bulk} justifies the downshift of the pseudo-Brewster angle. It is exactly what occurs in that experiment as the corresponding photon energy of the hydrogen Lyman alpha is ≈ 10.2 eV.

This study is qualitative. A quantitative analysis, which allows to determine the offset of the photon energy to trigger the downshift of the Brewster angle, the conductivity of graphene, and the functional relationship between the number of layers and the magnitude of the effect, requires a dedicated measurements campaign and a set of suitably grown samples that allows to explore the response as a function of the number of layers.

Before moving on to the study of the optical constants of graphene, we have to know that the materials exhibit a complex refractive index $\mathbf{n} = n + ik$ in the VUV–EUV spectral range. The terms n and k , real and imaginary parts of the refractive index, are usually experimentally derived by applying methods based on reflectance and transmittance measurements combined with optimized algorithms for data fitting analysis.^[46]

Figure 9 and Figure 10 show s- and p- experimental reflectance with the error bars of 1LG/SiO₂/Si (R_s black line and R_p blue line) and 3LG/SiO₂/Si (R_s black line and R_p blue line) samples. The curves, retrieved from the BEAR measurements, were fit

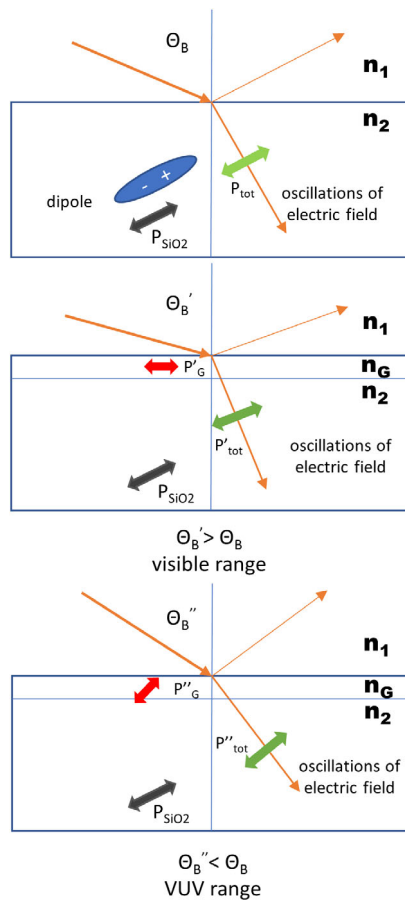


Figure 8. Pseudo-Brewster angle in case of uncoated bulk SiO₂/Si (TOP), graphene/SiO₂/Si structure in the visible spectral region (middle), and in the VUV spectral region (bottom). The arrows represent the classical emitting dipole components for bulk SiO₂, (black), for graphene film, (red), and the dipole component of the structure (green), resulting in the superposition of the contributions from the SiO₂ bulk and the surface layers.

using IMD software to estimate the optical constants of graphene.^[41] The IMD code takes into account parallel uniform layers of isotropic materials. The fitting procedure is based on the simulation of the sample structure by decomposing it into homogeneous layers corresponding to the various elements, materials, and compounds constituting the sample. In this case, from the bottom up to the surface exposed to the probing radiation, the layers are Si, SiO₂, and G, as shown in Figure 1. At each interface, the Fresnel coefficients for reflection and transmission of the incident fields, according to the polarization state of the electromagnetic (EM) wave, are recursively applied, whereas the thickness of each layer is taken into account as a phase propagation and amplitude factor. The fitting procedure can be relatively straightforward in the case of multilayer structures with thicknesses of a few nanometers. However, in case of graphene, the nearly atomic layer thickness and the atomic orbital structure of the film play a pivotal role for both interfaces and thickness. We know that by modeling graphene as a uniform homogeneous layer, we could derive only a sort of “effective refractive index”

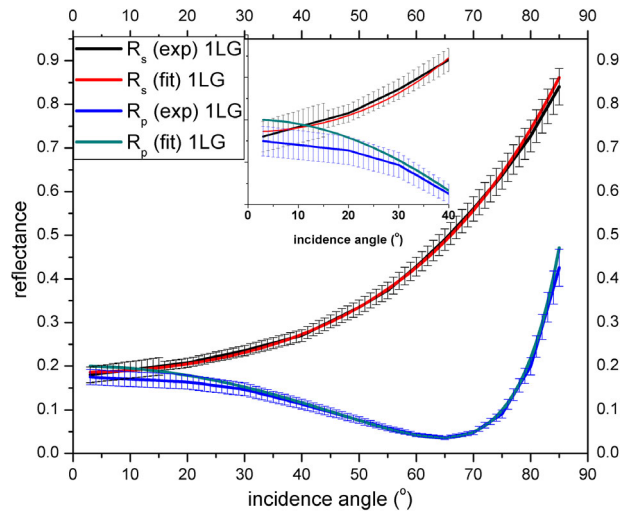


Figure 9. IMD-fitted curves and experimental data of s- and p-reflectance of 1LG/SiO₂/Si; the inset shows the zoom of the near-normal incidence region. Black and blue curves are the experimental R_s and R_p , respectively, red and green, and the corresponding IMD-fitted curves, assuming one set of n and k constants for the whole curve in each polarization. The inset shows large deviation of the fitted data from the experimental one in case of p-reflectance near-normal incidence.

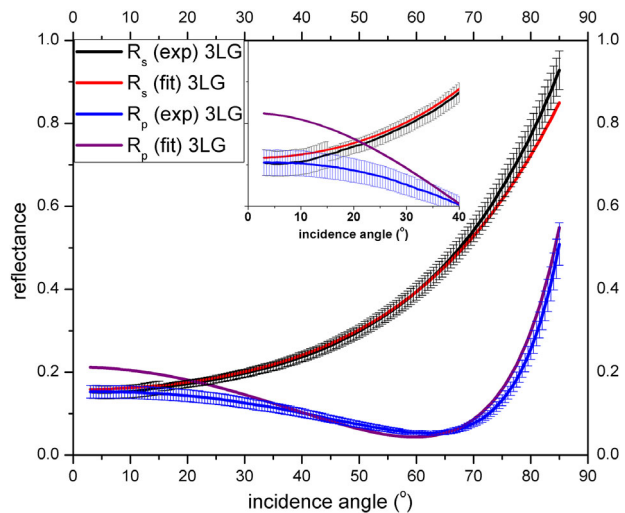


Figure 10. IMD-fitted curve and experimental data of s- and p-reflectance of 3LG/SiO₂/Si; the inset shows the zoom of the near-normal incidence region. Black and blue curves are the experimental R_s and R_p , respectively, red and purple, and the corresponding IMD-fitted curves, assuming one set of n and k constants for the whole curve in each polarization. The inset shows large deviation of the fitted data from the experimental one in case of p-reflectance near-normal incidence; however, from the figure it is clear that the best fit of the R_p curve is not well accomplished also for the other angles.

and “effective optical thickness” that are strictly interrelated and entangled. Furthermore, the roughness effects are included on those. The “effective refractive index” and “effective optical

constants” have been determined by fitting the experimental data, assuming a classical multilayer model consisting of Si substrate, a bulky layer (285 nm) of SiO₂, and a thin layer of graphene. The thickness of graphene ranges within 0.34–0.5 nm for 1LG and 1.4–1.7 nm for 3LG. The best assessment of these values of thickness was determined as a trade-off, combining the Raman results and indicating that the optical constants fit for s- and p-polarization at near-normal incidence should be nearly equal as they should not depend on the polarization state for small incidence angles. We used the optical constants reported in the study by Palik et al.^[47] for Si and those derived in some recent measurements of the same sample for SiO₂.^[39] Figure 9 and 10 show, together with the experimental curves, the fitted curves obtained by assuming a thickness derived from the mentioned trade off procedure, i.e., 0.34 nm for 1LG/SiO₂/Si and 1.7 nm for 3LG/SiO₂/Si. The reflectance data are well fitted in the whole angle range (3°–85°) in case of s-polarization. In case of p-polarized reflectance, the fitting procedure does not converge with the unique set of optical constants in the whole angular range. Particularly near-normal incidence p-reflectance fitting deviates significantly from the experimental data. This is shown in the insets of Figure 9 and 10 and it is true for any graphene thickness value within the ranges defined earlier. It is clear evidence of optical anisotropic behavior of graphene. As we know in the isotropic materials, the EM light propagation is independent of propagation direction within the medium as the dielectric constant and the refractive index are scalar quantities. However, in anisotropic optical materials, optical response changes with orientation of the sample or incidence angle of light. The dielectric constant and refractive index depend on the direction of propagation of the EM wave and the polarization direction of the wave electric field. For example, in the case of uniaxial anisotropy, the EM wave can be decomposed into ordinary and extraordinary waves. The ordinary wave follows Snell’s law and the material has constant refractive index, not dependent on direction of propagation. On the contrary, for the extraordinary wave, the uniaxial material has refractive index changing with the propagation direction according to the index ellipsoid. This is the case we face for graphene, where s- and p-electron bands generate a nonisotropic structure.^[48] These results suggest a change to approach the problem. Accordingly, the angular range was divided into several suitable smaller intervals, wide enough to allow reasonable confidence in the convergence of the fitting procedure to determine one pair of *n* and *k* for each angular segment. In case of the single-layer graphene, the angular segments identified were two; however, in the case of the trilayer graphene, seven angular segments were identified.

Figure 11 and 12 show only the p-experimental reflectance with the error bars and the fitted curves obtained by following the method described earlier.

The experimental data are well fitted for both samples. Table 2 shows the data obtained in the fit procedures for *n* and *k* as a function of light polarization and angular regions and summarizes what is qualitatively shown in Figure 11 and 12. The uncertainty associated with the values and shown in Table 2 is determined by taking into account the uncertainty of the graphene layer. Within the uncertainty, for small incidence angles and for both samples, *n_s*, *k_s*, and *n_p*, *k_p* do not depend on the light polarization as expected.

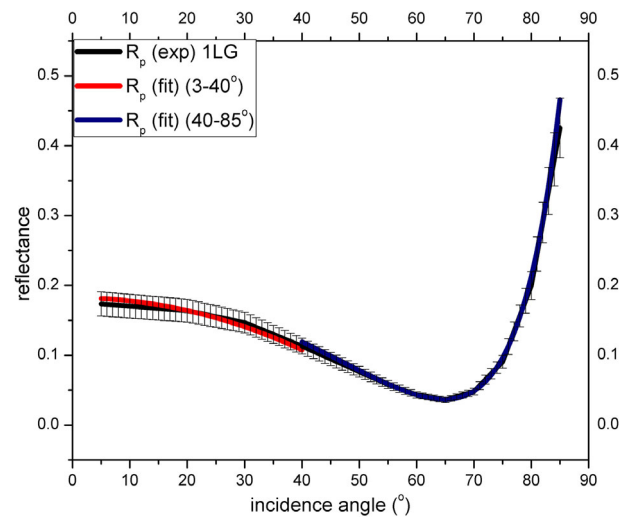


Figure 11. IMD-fitted curve and experimental data of p-reflectance of 1LG/SiO₂/Si with the error bars. The experimental curve is shown in black and colored curves correspond to the fitting for the *n* and *k* corresponding to various angular segments.

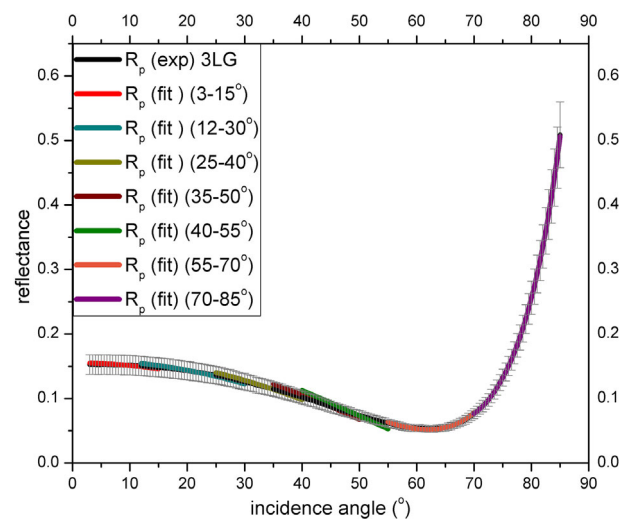


Figure 12. IMD-fitted curve and experimental data of p-reflectance of 3LG/SiO₂/Si with the error bars. The experimental curve is shown in black and colored curves correspond to the fitting for the *n* and *k* corresponding to various angular segments.

To the best of our knowledge, this is the first time that the experimental optical constants of few-layer graphene have been measured at hydrogen Lyman-alpha spectral line.

The surface-differential reflectance (SDR) measurement is a parameter often used to quantitatively estimate the effect of a very thin layer on top of an optical surface.^[49]

To derive reliable SDR measurements, a very critical and accurate sample preparation procedure has to be followed, obtaining finally representative samples for both coated and uncoated surfaces. This was not the present case; however, we thought that as the very thin graphene layer should affect mostly the sample surface properties instead of acting as a classical uniform layer,

Table 2. The real and imaginary parts (n , k) of monolayer and trilayer graphene in case of s- and p-polarized light.

Angular segment [°]	n_s	k_s	n_p	k_p
1LG				
3–40	2.65 ± 0.25	$<10^{-5}$	2.95 ± 0.25	$<10^{-5}$
40–85	2.65 ± 0.25	$<10^{-5}$	0.19 ± 0.05	0.62 ± 0.07
3LG				
3–15	2.48 ± 0.25	$<10^{-5}$	2.51 ± 0.14	$<10^{-5}$
12–30	2.48 ± 0.25	$<10^{-5}$	2.33 ± 0.11	$<10^{-5}$
25–40	2.48 ± 0.25	$<10^{-5}$	2.13 ± 0.09	$<10^{-5}$
35–50	2.48 ± 0.25	$<10^{-5}$	1.83 ± 0.05	$<10^{-5}$
45–60	2.48 ± 0.25	$<10^{-5}$	0.37 ± 0.04	0.64 ± 0.01
55–70	2.48 ± 0.25	$<10^{-5}$	0.51 ± 0.06	0.78 ± 0.01
70–85	2.48 ± 0.25	$<10^{-5}$	0.54 ± 0.06	0.82 ± 0.05

some sort of SDR qualitative measurements could be derived from the carried out measurements.

The SDR for s- and p-polarized light can be directly derived by the experimental reflectances using Equation (1) and (2).

$$(\text{SDR})_s = \left(\frac{\Delta R}{R}\right)_s = \frac{R_{sG} - R_{s\text{SiO}_2}}{R_{s\text{SiO}_2}} \quad (1)$$

$$(\text{SDR})_p = \left(\frac{\Delta R}{R}\right)_p = \frac{R_{pG} - R_{p\text{SiO}_2}}{R_{p\text{SiO}_2}} \quad (2)$$

where, R_{sG} , R_{pG} are the s- and p-reflectance of the sample coated with graphene and $R_{s\text{SiO}_2}$ and $R_{p\text{SiO}_2}$ are the s- and p-reflectance of bare substrate, respectively.

The theoretical SDR for s- and p-polarized light can be estimated by the relationships presented in various studies,^[50,51] respectively, that are based on the ultrathin approximation of films and directly depend on the optical constants. We used the retrieved optical constants values to calculate the theoretically estimated SDR using the relationships presented in the aforementioned studies.

Figure 13 and **14** show the 1 L graphene experimental SDR_s and SDR_p together with the calculated trends calculated using the retrieved optical constants shown in Table 2 and the relationships reported in various studies.^[50,51]

Similarly, **Figure 15** and **16** show the same comparison for 3LG graphene sample. Taking into account the fact that the samples were not properly prepared for SDR measurements and that the derived optical constants are only “effective” as it was not possible to unequivocally distinguish the thickness and the refractive index within the adopted approximation, we can conclude that the results clearly confirm how graphene affects the optical properties of the sample surface.

4. Conclusion

Optical properties of 1LG and 3LG over dielectric substrate were investigated experimentally at hydrogen Lyman-alpha spectral line. The optical performance of the graphene samples over

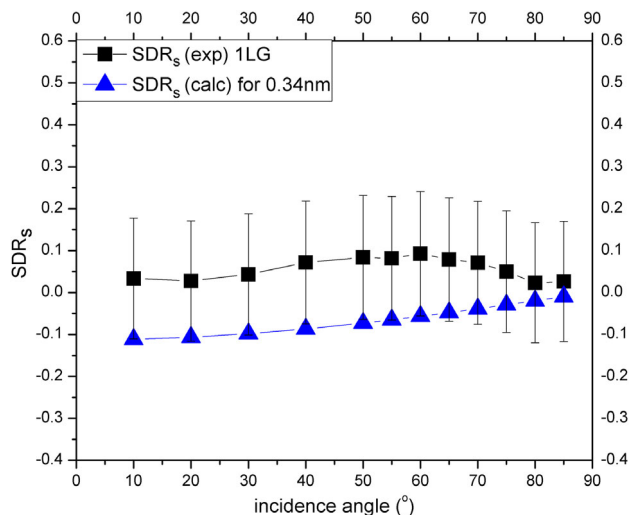


Figure 13. Comparison of 1LG $(\text{SDR})_s$ experimental and $(\text{SDR})_s$ calculated theoretically using the experimentally retrieved optical constants. Experimental data with error bars are represented in black and the calculated data in blue.

the dielectric substrate (SiO_2) was studied in terms of reflectance, pseudo-Brewster angle, and optical constants of graphene layers. Optical anisotropy with the axis of symmetry nearly perpendicular to the surface and coherently related to the p-orbital structural orientation has been demonstrated for the first time at 121.6 nm. In contrast to the literature, a novel downshift of the pseudo-Brewster angle due to graphene was reported and discussed in detail. Anisotropic “effective optical constants” corresponding to the effective thickness of both samples of graphene (1LG and 3LG) were determined for the first time to the best of our knowledge. Furthermore, the retrieved optical parameters were

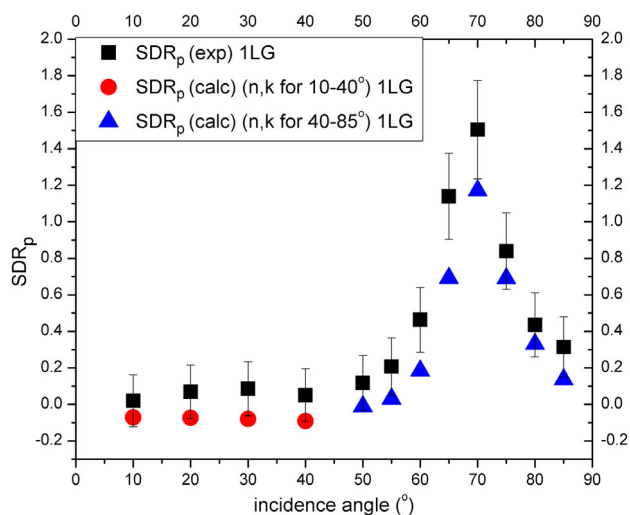


Figure 14. Comparison of 1LG $(\text{SDR})_p$ experimental and $(\text{SDR})_p$ calculated using the retrieved optical constants corresponding to the defined angular segments of the reflectance data. Experimental data with error bars are represented in black and the calculated data for each angular segment are represented in different colors.

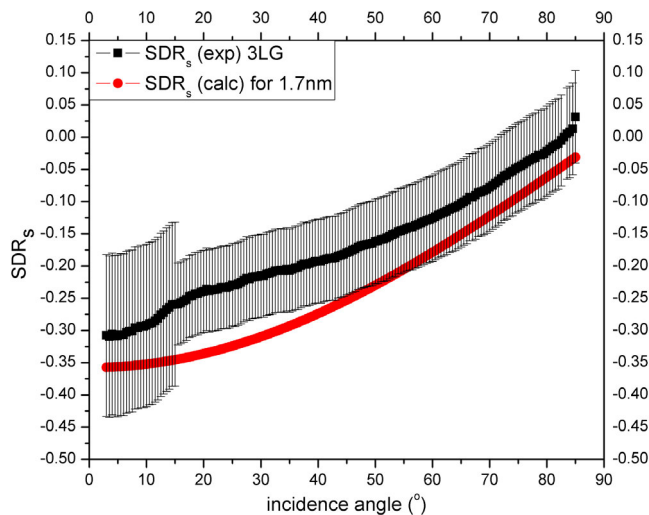


Figure 15. Comparison of 3LG $(SDR)_s$ experimental and $(SDR)_s$ calculated theoretically using the retrieved optical constants. Experimental data with error bars are represented in black and the calculated data in red.

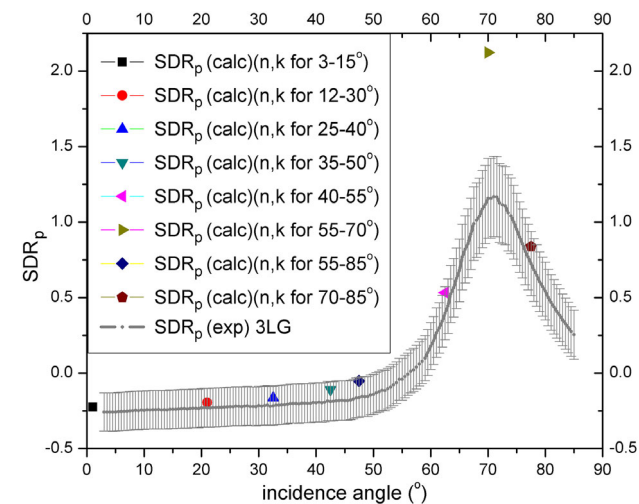


Figure 16. Comparison of 3LG $(SDR)_p$ experimental and $(SDR)_p$ calculated using the retrieved optical constants corresponding to the defined angular segments of the reflectance data. Experimental data with error bars are represented in grey and the calculated data for each angular segment are represented in different colors.

qualitatively analyzed using surface differential reflectance analysis. This is the first experimental optical analysis of graphene at VUV spectral region, which can open up new prospective applications and utilization of it for space instrumentation, advanced lithography systems, etc.

Acknowledgements

This research project was supported by the Education, Audiovisual and Culture Executive Agency (EACEA) Erasmus Mundus Joint Doctorate, project no. 2012–0033. The first author is part of the EXTATIC Program.

The authors express special gratitude to Professor S. Nannarone, Professor Luca Pasquali, and Dr. Kostantin Koshmak as a team at BEAR beamline-ELETTRA (Trieste). The measurements at BEAR were carried out in the frame of the proposals 20170269 and 20180427.

Conflict of Interest

The authors declare no conflict of interest.

Data Availability Statement

Research data are not shared.

Keywords

graphene, hydrogen Lyman alpha, optical constants, pseudo-Brewster angles, vacuum ultraviolet optical anisotropy

Received: December 29, 2020

Revised: February 5, 2021

Published online: May 2, 2021

- [1] Y. H. Wu, T. Yu, Z. X. Shen, *J. Appl. Phys.* **2010**, *108*, 1.
- [2] A. H. C. Neto, K. Novoselov, *Rep. Prog. Phys.* **2011**, *74*, 082501.
- [3] Y. Zhang, Y. W. Tan, H. L. Stormer, P. Kim, *Nature* **2005**, *438*, 201.
- [4] S. Chen, L. Brown, M. Levendorf, W. Cai, S.-Y. Ju, J. Edgeworth, X. Li, C. W. Magnuson, A. Velamakanni, R. D. Piner, J. Kang, J. Park, R. S. Ruoff, *ACS Nano* **2011**, *5*, 1321.
- [5] N. T. Kirkland, T. Schiller, N. Medhekar, N. Birbilis, *Corros. Sci.* **2012**, *56*, 1.
- [6] J. S. Bunch, S. S. Verbridge, J. S. Alden, A. M. Van Der Zande, J. M. Parpia, H. G. Craighead, P. L. McEuen, *Nano Lett.* **2008**, *8*, 2458.
- [7] V. Mišković-Stanković, I. Jevremović, I. Jung, K. Rhee, *Carbon* **2014**, *75*, 335.
- [8] P. Zuppella, F. Gerlin, M. G. Pelizzo, *Opt. Mater.* **2017**, *67*, 132.
- [9] F. J. Nelson, V. K. Kamineni, T. Zhang, E. S. Comfort, J. U. Lee, A. C. Diebold, *Appl. Phys. Lett.* **2010**, *97*, 1.
- [10] R. R. Nair, P. Blake, A. N. Grigorenko, K. S. Novoselov, T. J. Booth, T. Stauber, N. M. R. Peres, A. K. Geim, *Science* **2008**, *320*, 1308.
- [11] X. Wang, Y. P. Chen, D. D. Nolte, *Opt. Express* **2008**, *16*, 22105.
- [12] M. Bruna, S. Borini, *Appl. Phys. Lett.* **2009**, *94*, 2007.
- [13] Z. H. Ni, H. M. Wang, J. Kasim, H. M. Fan, T. Yu, Y. H. Wu, Y. P. Feng, Z. X. Shen, *Nano Lett.* **2007**, *7*, 2758.
- [14] A. Gray, M. Balooch, S. Allegret, S. De Gendt, W. E. Wang, *J. Appl. Phys.* **2008**, *104*, 053109.
- [15] J. W. Weber, V. E. Calado, M. C. M. Van De Sanden, *Appl. Phys. Lett.* **2010**, *97*, 1.
- [16] J. Gong, R. Dai, Z. Wang, C. Zhang, X. Yuan, Z. Zhang, *Mater. Res. Express* **2017**, *4*, 085005.
- [17] H. Savaloni, M. Firouzi-Arani, *Philos. Mag.* **2008**, *88*, 711.
- [18] A. E. H. Gaballah, P. Zuppella, N. Ahmed, K. Jimenez, G. Pettinari, A. Gerardino, P. Nicolosi, in *EUV and X-Ray Optics: Synergy Between Laboratory and Space V* (Eds: R. Hudec, L. Pina), SPIE, Bellingham, WA **2017**, p. 102350X.
- [19] A. Giglia, *BEAR Beamline Description. Elettra Sincrotrone Trieste*, <https://www.elettra.trieste.it/it/lightsources/elettra/elettra-beamlines/bear/beamline-description.html>.

- [20] S. Nannarone, F. Borgatti, A. Deluisa, B. P. Doyle, G. C. Gazzadi, A. Giglia, P. Finetti, N. Mahne, L. Pasquali, M. Pedio, G. Selvaggi, G. Nalletto, M. G. Pelizzo, G. Tondello, in *AIP Conf. Proc.*, **2004**, pp. 450–453.
- [21] Graphenea, Monolayer Graphene on 300 nm SiO₂/Si, <https://www.graphenea.com/collections/buy-graphene-films/products/monolayer-graphene-on-sio2-si-4-wafer>.
- [22] F. Bonaccorso, J. Coraux, C. Ewels, G. Fiori, A. C. Ferrari, J-C. Gabriel, M. Garcia-Hernandez, J. Kinaret, M. Lemme, D. Neumaier, V. Palermo, A. Zenasni, S. Roche, *Graphene Position Paper E-nano Newsletter*, <http://www.phantomsnet.net/nanoICT/ppapers.php>.
- [23] C. Casiraghi, A. Hartschuh, E. Lidorikis, H. Qian, H. Harutyunyan, T. Gokus, K. S. Novoselov, A. C. Ferrari, *Nano Lett.* **2007**, *7*, 2711.
- [24] P. Blake, E. W. Hill, A. H. Castro Neto, K. S. Novoselov, D. Jiang, R. Yang, T. J. Booth, A. K. Geim, *Appl. Phys. Lett.* **2007**, *91*, 063124.
- [25] J. Kim, F. Kim, J. Huang, *Mater. Today* **2010**, *13*, 28.
- [26] B. Pacakova, J. Vejpravova, A. Repko, A. Mantlikova, M. Kalbac, *Carbon* **2015**, *95*, 573.
- [27] Park Systems, *Atomic Force Microscopy Systems AFM System*, Park Systems **2017**.
- [28] C. Casiraghi, A. Hartschuh, E. Lidorikis, H. Qian, H. Harutyunyan, T. Gokus, K. S. Novoselov, A. C. Ferrari, *Nano Lett.* **2007**, *7*, 2711.
- [29] F. Tuinstra, J. L. Koenig, *J. Chem. Phys.* **1970**, *53*, 1126.
- [30] A. C. Ferrari, J. C. Meyer, V. Scardaci, C. Casiraghi, M. Lazzeri, F. Mauri, S. Piscanec, D. Jiang, K. S. Novoselov, S. Roth, A. K. Geim, *Phys. Rev. Lett.* **2006**, *97*, 1.
- [31] S. Ryu, J. Maultzsch, M. Y. Han, P. Kim, L. E. Brus, *ACS Nano* **2011**, *5*, 4123.
- [32] A. C. Ferrari, *Solid State Commun.* **2007**, *143*, 47.
- [33] Y. A. Kim, K. Fujisawa, H. Muramatsu, T. Hayashi, M. Endo, T. Fujimori, K. Kaneko, M. Terrones, J. Behrends, A. Eckmann, C. Casiraghi, K. S. Novoselov, R. Saito, M. S. Dresselhaus, *ACS Nano* **2012**, *6*, 6293.
- [34] H. Park, J. A. Rowehl, K. K. Kim, V. Bulovic, J. Kong, *Nanotechnology* **2010**, *21*, 505204.
- [35] M. S. Dresselhaus, A. Jorio, R. Saito, *Annu. Rev. Condens. Matter Phys.* **2010**, *1*, 89.
- [36] N. Fairley, C. S. Ltd, *CasaXPS Manual 2.3.15: CasaXPX Processing Software for XPS Spectra*, Casa Software Limited **2009**.
- [37] H. Sjuts, *Dr. Sjuts Optotechnik GmbH–Channel Electron Multipliers and Complete Measurement Systems*, Dr. Sjuts Optotechnik GmbH. http://www.sjuts.com./CEMModels_Standard.html.
- [38] A. E. H. Gaballah, P. Nicolosi, N. Ahmed, K. Jimenez, G. Pettinari, A. Gerardino, P. Zuppella, *Appl. Surf. Sci.* **2019**, *463*, 75.
- [39] N. A. Malik, P. Nicolosi, A. E. H. Gaballah, K. Jimenez, P. Zuppella, in *EUV and X-ray Optics: Synergy between Laboratory and Space VI*, (Eds: R. Hudec, L. Pina), SPIE, Bellingham, WA **2019**, p. 32.
- [40] A. E. H. Gaballah, P. Nicolosi, N. Ahmed, K. Jimenez, G. Pettinari, A. Gerardino, P. Zuppella, *Rev. Sci. Instrum.* **2018**, *89*, 015108.
- [41] D. L. Windt, *Comput. Phys.* **1998**, *12*, 360.
- [42] S. Glen, *Error Propagation (Propagation of Uncertainty)*, <https://www.statisticshowto.com/error-propagation/>.
- [43] C. Mi, S. Chen, W. Wu, W. Zhang, X. Zhou, X. Ling, W. Shu, H. Luo, S. Wen, *Opt. Lett.* **2017**, *42*, 4135.
- [44] B. Majérus, M. Cormann, N. Reckinger, M. Paillet, L. Henrard, P. Lambin, M. Lobet, *2D Mater.* **2018**, *5*, 025007.
- [45] A. G. Marinopoulos, L. Reining, A. Rubio, V. Olevano, *Phys. Rev. B* **2004**, *69*, 245419.
- [46] W. R. Hunter, *Appl. Opt.* **1982**, *21*, 2103.
- [47] E. Palik, *Handbook of Optical Constants of Solids*, Academic Press, USA **1998**.
- [48] C. C. Davis, in *Lasers and Electro-Optics*, Cambridge University Press, Cambridge **2014**, pp. 539–579.
- [49] H. Proehl, R. Nitsche, T. Diemel, K. Leo, T. Fritz, *Phys. Rev. B* **2005**, *71*, 165207.
- [50] P. Adamson, *Appl. Opt.* **2017**, *56*, 7832.
- [51] J. D. E. McIntyre, D. E. Aspnes, *Surf. Sci.* **1971**, *24*, 417.